PUBLICATION [P4]

Analysis of Leakages in a Solid Oxide Fuel Cell Stack in a System Environment

In: Fuel Cells
Article first published online 16th March 2015

DOI: 10.1002/fuce.201400072

Analysis of Leakages in a Solid Oxide Fuel Cell Stack in a System Environment

M. Halinen[1]*, J. Pennanen[1]

[1] VTT Technical Research Centre of Finland, P.O. Box 1000, FI-02044, VTT, Finland

Received April 25, 2014; accepted November 05, 2014; published online ■■■

Abstract

A solid oxide fuel cell (SOFC) stack can exhibit both anodic and cathodic leakages, i.e. a fuel leak from the anode side and an air leak from the cathode side of the stack, respectively. This study describes the results of an in-situ leakage analysis conducted for a planar SOFC stack during 2000 hours of operation in an actual system environment. The leakages are quantified experimentally at nominal system operating conditions by conducting composition analysis and flow metering of gases for both fuel and air subsystems. Based on the calculated atomic hydrogen-to-carbon ratio of the fuel and air gases, it is found that the fuel leakages are mostly selective by nature: the leaking fuel gas does not have the same composition as the fuel system gas. A simple diffusive leakage model, based on the leakage being driven by concentration differences weighted by diffusion coefficients, is applied to quantify the amount of leakages. The leakage model provides a good correspondence with the experimental results of the gas analysis.

Keywords: Diagnosis, Experimental Results, Fuel Cell System, Leakage, Mass Transport, Solid Oxide Fuel Cell, Stack, Testing

1 Introduction

Solid oxide fuel cells (SOFCs) are electrochemical devices operating at a high temperature. SOFCs have several benefits, such as high efficiency, low emissions, and fuel flexibility, which make them an attractive technology for distributed power generation, auxillary power units (APUs), and various other applications. A planar SOFC stack requires a gas-tight electrolyte as well as high-temperature seals between the different stack components, to prevent harmful mixing of the anode fuel gas (typically reformed gaseous hydrocarbons) and cathode oxidant gas (typically ambient air). Thus, sufficient gas-tightness is required to realize a working and robust SOFC stack, and there are many different techniques and materials developed to achieve this goal [1]. However, experimental work has shown that an SOFC can have both internal leakages between the anode and cathode, e.g. through the electrolyte as well as external leakages between the SOFC and surroundings [2, 3]. Therefore, an SOFC may exhibit a certain characteristic and admissible amount of leakages, which has to be taken into account in the design and operation of SOFC stacks and systems.

In a complete SOFC system, the stack leakages affect the system design, since the leakage can alter the heat production between the different system components. For example, if leakages cause oxidation of a larger amount of the fuel gas already in the stack, then a smaller amount of fuel is fed to the burner downstream of the SOFC stack, thus decreasing the outlet temperature of the burner. Concurrently, there is more heat production in the SOFC stack than is the case without leakages. Moreover, in systems with anode off-gas recycling (AOGR), leakages can create adverse effects during system heat-up and cool-down cycles, and can compromise safe operation of the system [4]. Naturally, leakages mean that less fuel than intended is fed to the anode, thus increasing the fuel utilization of the stack, which can lead to fuel starvation and anode oxidation [5]. Therefore, information on the leakages is relevant and even crucial for various aspects of SOFC system design and operation.

The leakages may be driven by the pressure and concentration differences present between the anode and cathode sides of the stack [2, 5]. A viscous leakage, driven by a pressure difference, has the same composition as the respective bulk gas flowing at the anode or cathode. A diffusive leakage, driven by the concentration difference, does not necessarily have the same composition as the bulk gas, since the composition of such a leak depends on the diffusivity of various substances in the bulk gas. The diffusion mass transport mechanism is relevant especially for fuel gas leakages, since the gas components, such as hydrogen and steam, have large differences in their molecular size. Regardless of the dominating mass transport mechanism, the leakage changes the composition of fuel and air system gases in a similar manner: fuel leaking into an air system combusts to carbon dioxide and steam, while air leaking into a fuel system will oxidize flammable substances of the fuel gas. The nature and quantity of the leakages can be investigated by measuring the changes they make to the com-

[*] *Corresponding author, matias.halinen@gmail.com*

position of the bulk gas, and this approach is used in this study as well.

Online and *in situ* methods to detect or quantify any changes in stack leakages could potentially be used for system fault diagnostics and to evaluate the mechanisms causing stack degradation. Increased stack leakages induce voltage degradation and temperature increases in the stack. Quantification of any changes in the stack leakages during operation would thus be beneficial for distinguishing them from other reasons causing stack voltage degradation, such as an increase in contact resistance, or system faults such as sulphur poisoning or measurement errors. Prior to this study, leakages have been investigated extensively by *ex situ* testing of different materials used as seals for stacks [1], and also by simulations for complete stack aggregates [5], as well as experimentally in single cell test stands [2]. However, to the authors' knowledge, no studies have been published previously on the quantification of leakages for complete stacks operated in an actual system environment.

In this study, a method is presented to: (i) identify the prevailing mass-transport phenomenon causing the anodic leakages; and (ii) quantify the anodic and cathodic leakages. The method is applied for an SOFC stack operated in an actual system environment at nominal operating conditions. The experimental setup and the basis of the analysis method – the use of measurements for both fuel and air systems, together with simple leakage models for diffusive and viscous mass-transport phenomena – are described in Section 2. In Section 3, the composition of the fuel and air systems' gases is determined experimentally, and the prevailing mass-transport mechanism of anodic leakage is identified. Finally, the effects of the leakages on selected characteristics related to the system design and operation are presented and discussed.

2 Experimental

2.1 10 kW SOFC Demonstration Unit

The experiments were conducted with a planar SOFC stack operated in a 10 kW SOFC system at VTT Technical Research Centre of Finland. The 10 kW SOFC system consists of two interconnected modules, the balance of plant (BoP) and the stack module. It utilises an AOGR loop, which enables system operation without an external steam supply when the stack current and single-pass fuel utilization are high enough. Ambient air is fed into the system with a blower and filtered with a particle filter. Other system components include heat exchangers, a catalytic burner, and a reformer to maintain the thermal balance of the system and stack during operation [6].

The SOFC stack was designed, manufactured, and installed in the 10 kW SOFC system by Versa Power Systems (VPS), and it consisted of 64 planar anode supported cells with 550 cm^2 of active area each, and cross-flow geometry for fuel and air gases [7]. The SOFC stack is located inside a thermally insulated and gas-tight module designed by VPS. Inlet air fed to the module flushes the module internal space around the stack before it is forced into cathode inlet air manifolds and through the stack, an arrangement known as air inlet flush (Figure 1). Fuel and cathode outlet gases flow in separate pipes connected to the stack manifold.

The experimental results presented in this study were recorded during a 2,000 h test run, during which the system was operated constantly at the same nominal operating conditions with a stack current of 200 A, an air flow rate of 973 NLPM, a natural gas flow rate of 27.9 NLPM, and a recycle flow rate of 174.7 NLPM. The pressure difference between the anode and cathode of the stack was below 15 hPa at said nominal operating conditions. The pressure was measured from the stack inlet and outlet manifolds.

2.2 Leakage Definitions

As described above, an SOFC stack can exhibit leakages, e.g. through the electrolyte and various interfaces between different parts of the stack assembly. Figure 1 illustrates possible routes for gas leaks taken into account for a planar cross-flow SOFC stack in a gas-tight module with air inlet flush flow configuration. Fuel leakages from the anode side of the stack and from fuel manifolds are called *anodic leakages*, and air leakages from the SOFC cathode side and air manifolds are called *cathodic leakages*. It is evident that there are many possible

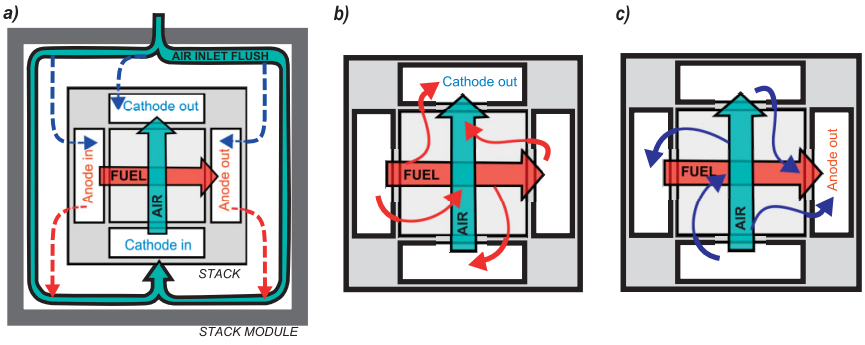

Fig. 1 Valid leakage routes for: a) external anodic (*Aext*) and cathodic (*Cext*) leakages, b) internal anodic (*Aint*) leakages, and c) internal cathodic (*Cint*) leakages.

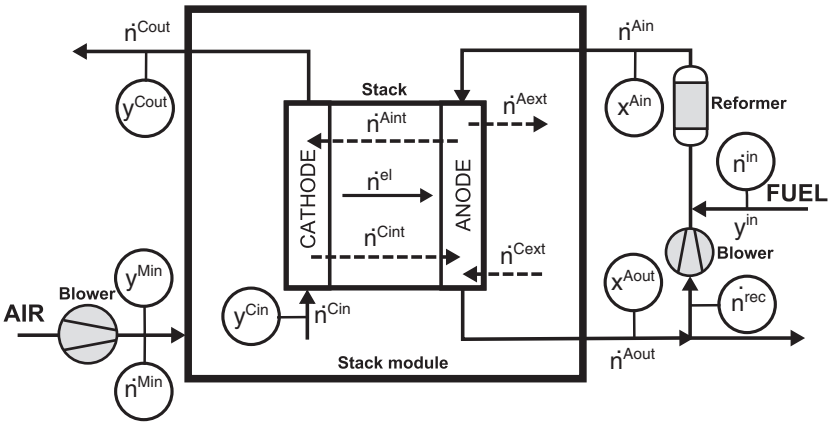

Fig. 2 Experimental setup. Anodic and cathodic leakages are marked with dashed lines. Other system mass flows (air and fuel gas, as well as transport of oxygen) are marked with solid lines. Measured variables are denoted with circles.

interfaces for the leakages to occur, but both the anodic and cathodic leakages can be differentiated from internal and external leakages as follows:

(i) *External leakages* (Figure 1a) occur between the gas manifolds and the module air inlet flush e.g. through manifold seals. Due to the air inlet flush, anodic external leakages are fed into the cathode inlet and, after passing through the stack, end up at the cathode outlet manifold.

(ii) *Internal leakages* (Figure 1b–c) occur inside the stack and between the inlet and outlet manifolds, e.g. through the electrolyte or stack seals. Any anodic internal leakages end up at the cathode outlet manifold (Figure 1b). Similarly, any cathodic internal leakages end up at the anode outlet manifold (Figure 1c).

Due to the many possible leakage paths, the composition of the leakage may not be a single value. The composition depends on the location of the leakage at the various interfaces in the stack, where chemical and electrochemical reactions constantly alter the gas composition according to prevailing conditions (see e.g. [8] for details). However, any leakages depicted in Figure 1a-c mix with a significantly larger amount of bulk gas, fuel, or air, flowing through the anode and cathode and around the stack as air inlet flush. Additionally, due to the high operating temperature and the presence of catalytically active materials, it is expected that reactions occur between the leakages and the bulk gases according to Eqs. (1)–(3). Flammable substances in an anodic leakage react with oxygen and are combusted to CO_2 and H_2O at the cathode side. Similarly, oxygen in a cathodic leakage reacts with fuel gas at the anode side.

$$CH_4 + 2O_2 \rightarrow CO_2 + 2H_2O \quad (1)$$

$$CO + 1/2\ O_2 \rightarrow CO_2 \quad (2)$$

$$H_2 + 1/2\ O_2 \rightarrow H_2O \quad (3)$$

Since the individual leakages mix and react with a larger amount of bulk gas, this study does not try to model or quantify any spatially distributed individual leakages of the stack. Instead of the individual leakage routes illustrated in Figure 1a–c, this study considers the leakages in a form in which the total amounts of the leakages ($\dot{n}^{Atot}$ and $\dot{n}^{Ctot}$) are expressed as flow rates, where:

$\dot{n}^{Atot}$ is the sum of anodic leakages $\dot{n}^{Aext} + \dot{n}^{Aint}$, where

- $\dot{n}^{Aext}$, anodic external leakage, is the total amount of fuel leaking from the anode inlet and outlet manifolds to the air inlet flush, as depicted in Figure 1a.
- $\dot{n}^{Aint}$, anodic internal leakage, is the total amount of fuel leaking from anode to cathode air flow, as depicted in Figure 1b.

$\dot{n}^{Ctot}$ is the sum of cathodic leakages $\dot{n}^{Cext} + \dot{n}^{Cint}$, where

- $\dot{n}^{Cext}$, cathodic external leakage, is the total amount of air leaking from the air inlet flush to the stack fuel manifolds, as depicted in Figure 1a.
- $\dot{n}^{Cint}$, cathodic internal leakage, is the total amount of air leaking from cathode to anode fuel flow, as depicted in Figure 1c.

2.3 Measurements

The experimental setup used in this study to detect and quantify the leakages $\dot{n}^{Ctot}$ or $\dot{n}^{Atot}$ is depicted in Figure 2, and the description of the measured process variables denoted with circles is given in Table 1. In the air subsystem, the fractions of CO_2, H_2O, and O_2 in the cathode air were continuously sampled and measured at module inlet (y^{Min}), cathode inlet (y^{Cin}), and cathode outlet (y^{Cout}). Anodic leakages are detected by observing the changes in the measured gas composition between the sampling locations according to Eqs. (1)–(3). Additionally, measurements with FTIR and GC were conducted for *Cin* and *Cout* gas to ensure that anodic leakage is completely combusted to CO_2 and H_2O. The module inlet air ($\dot{n}^{Cin}$) flow rate was measured with a thermal mass flow meter.

Table 1 The measured variables and their uncertainty.

Measurement	Variable	Uncertainty
Natural gas	$\dot{n}^{in}$	±1% of value
Module inlet air	$\dot{n}^{Min}$	±3% of value
Recycle gas	$\dot{n}^{rec}$	±3% of value
Composition of humid air at *Min*, *Cin*, and *Cout*	y_{H_2O}	±450 ppm
	y_{CO_2}	±(5 ppm + 2% of value)
	y_{O_2}	±(0.2%-units + 2% of value)
Composition of dried fuel gas at *Ain* and *Aout*	x_{CH_4}, x_{CO}, x_{CO_2} x_{H_2}, x_{O_2}, $x_{N_2}x_{C_nC_m}$	±3% of value

A more complex arrangement is required for the fuel subsystem, to detect and quantify the flow rate and composition (y_j) of the gases flowing in the fuel system on a wet basis. Complexity arises because the humid fuel gas was cooled down to 2–3 °C to condensate the water vapour from the gas samples, and the gas analysis was done on a dry basis (x_i). From the dried fuel gas, CH_4, CO, CO_2, H_2, N_2, C_xH_y compounds up to C_5 hydrocarbons, and O_2/Argon were analyzed with GCs. The composition was analysed from periodically extracted gas samples at anode inlet (x^{Ain}) and anode outlet (x^{Aout}). A portion of the anode outlet gas (x^{Aout}) is recycled back into the system inlet, thus the recycling gas (x^{rec}) has the same composition. Composition of the fuel at the system inlet (y^{in}), high-grade natural gas from the Finnish gas grid, used in the experiment was not directly measured due to its stable composition, consisting of more than 98% methane and other hydrocarbons (Table 2). The inlet natural gas ($\dot{n}^{in}$) flow rate was measured with a thermal mass flow meter, and the recycle gas flow ($\dot{n}^{rec}$) with a turbine meter.

2.4 Leakage Analysis

2.4.1 Approach

It is clear that quantification of $\dot{n}^{Ctot}$ or $\dot{n}^{Atot}$, depicted in Figure 2, with any direct physical measurement devices would be extremely challenging to realize in an actual system environment due to, e.g. the high temperature of the gases and various reactions within the SOFC, affecting the composition as well as the molar flow of both the bulk gases and the leakages. Thus, the experimental setup for leakage analysis is based on the fact that leakages will change the flux of the elements, $\dot{n}_e$, $e = C, H, O, N$, between the inlet and the outlet of the anode and cathode of the stack, according to Eqs. (4) and (5), respectively.

Table 2 Average composition of system inlet fuel (natural gas) and uncertainty.

Substance	Variable	Average	Uncertainty
Methane	$y^{in}_{CH_4}$	97.9 mol-%	±1.0 mol-%
Ethane	$y^{in}_{C_2H_6}$	0.8 mol-%	±0.5 mol-%
Propane	$y^{in}_{C_3H_8}$	3,000 ppm	±2,000 ppm
Butane	$y^{in}_{C_4H_{10}}$	1,000 ppm	±600 ppm
Nitrogen	$y^{in}_{N_2}$	1 mol-%	±0.5 mol-%

$$\dot{n}_e^{Aout} = \dot{n}_e^{Ain} - \dot{n}_e^{Atot} + \dot{n}_e^{Ctot} + \dot{n}_O^{el} \quad (4)$$

$$\dot{n}_e^{Cout} = \dot{n}_e^{Min} + \dot{n}_e^{Atot} - \dot{n}_e^{Ctot} - \dot{n}_O^{el} \quad (5)$$

In Eq. (4), $\dot{n}^{Ctot}$ leakage supplies additional O and N to the fuel system gas, which consists mostly of substances containing the elements H and C – the main constituents of the inlet natural gas. Similarly, $\dot{n}^{Atot}$ in Eq. (5) supplies additional H and C to the air system, where any indigenous flux of these elements originates from the inlet ambient air as H_2O and CO_2, respectively. Flux of O through the electrolyte is denoted as $\dot{n}_O^{el}$.

The flux of elements takes place as a flow of the substances in the fuel and air system gases. Thus, the element flux at any process location can be determined based on the molar fractions of each substance containing the given element, and the total flow rate of the gas according to Eqs. (6) and (7).

$$\dot{n}_e = Y_e \dot{n} \quad (6)$$

$$Y_e = \sum_j A_{e,j} y_j \quad (7)$$

For example, for H, Eq. (7) is $Y_H = 4y_{CH4} + 2y_{H2} + 2y_{H2O} + my_{CnHm}$. Now, Eqs. (4) and (5) can be derived using Eqs. (6) and (7) as (8) and (9):

$$\dot{n}^{Aout} Y_e^{Aout} = \dot{n}^{Ain} Y_e^{Ain} - \dot{n}^{Atot} Y_e^{Atot} + \dot{n}^{Ctot} Y_e^{Ctot} + \dot{n}_O^{el} \quad (8)$$

$$\dot{n}^{Cout} Y_e^{Cout} = \dot{n}^{Min} Y_e^{Min} + \dot{n}^{Atot} Y_e^{Atot} - \dot{n}^{Ctot} Y_e^{Ctot} - \dot{n}_O^{el} \quad (9)$$

It should be noted that Eqs. (6)–(9) contain practically measurable process variables, i.e. molar fractions of substances and flow rates at various process locations (see Figure 2), which enable *in situ* leakage analysis of an SOFC stack while operated in an actual system environment. However, it becomes clear when looking into Eqs. (6)–(9) that the composition of the anodic leakage y^{Atot} is required to quantify the leakages. Since y^{Atot} cannot be measured directly, two simple leakage models based on different mass-transport phenomena, viscous and diffusive, are considered in the next chapters, to calculate the composition y^{Atot}.

2.4.2 Viscous Leakage

The composition ($y^{Atot,visc}$) of a viscous leakage, driven by the pressure difference between the anode and cathode sides of the stack, is assumed simply to be identical to the fuel gas composition at the SOFC anode, as in Eq. (10).

$$y_j^{Atot,visc} = y_j^{anode}, \text{ where } y^{anode} = y^{Ain}, y^{Aout} \quad (10)$$

The composition of y^{anode} is approximated with a single value by using either y^{Ain} or y^{Aout}. y^{Ain} and y^{Aout} are selected as representative values for y^{anode} since they represent the two extremes of the gas distribution within the SOFC stack [8], and they are calculated using the fuel system's measurements according to Appendix A.

The total cathodic leakage $\dot{n}^{Ctot}$ is assumed to occur viscously at all times, having an idealised composition of 21 vol-% of O_2 and 79 vol-% of N_2. The simplification is reasonable, since the amount of carbon dioxide and water vapour in $\dot{n}^{Ctot}$ is very small and has a negligible effect on the results.

2.4.3 Diffusive Leakage

The composition $\left(y^{Atot,diff}\right)$ of a diffusive leakage, driven by the difference in concentration between the anode and cathode sides of the stack, is approximated by weighting the molar fraction of substances in the fuel gas at the SOFC anode by their relative binary diffusion coefficients, using Eq. (11).

$$y_j^{Atot,diff} = \frac{D_j^{air}}{\sum_j D_j^{air} y_j^{anode}} \left(y_j^{anode} - y_j^{cathode}\right) \approx \frac{D_j^{air}}{\sum_j D_j^{air} y_j^{anode}} \left(y_j^{anode}\right), \quad \text{where } y^{anode} = y^{Ain}, y^{Aout} \tag{11}$$

D_j^{air} are the binary diffusion coefficients of each substance in air, estimated according to Fuller et al. [9]. The simplification to use only the composition of the fuel gas is reasonable, since $y_j^{anode} \gg y_j^{cathode}$ for CH_4, CO, CO_2, H_2, and H_2O components. Similarly, it is reasoned that no nitrogen or oxygen are leaking diffusively from anode to cathode, since $y_{N_2}^{anode} \ll y_{N_2}^{cathode}$ and $y_{O_2}^{anode} = 0$, respectively.

2.4.4 Distinction between Viscous and Diffusive Leakage

The anodic leakage will introduce an additional flux of C and H-containing substances into the air system. As long as the compounds that contain the elements C and H are oxidized completely, according to Eqs. (1)–(3), these element fluxes can be expressed as Eqs. (12) and (13).

$$\dot{n}_C^{Atot(ox)} = \dot{n}_C^{Cout} - \dot{n}_C^{Min} + \dot{n}_C^{Ctot} \approx \dot{n}^{Cout} y_{CO_2}^{Cout} - \dot{n}^{Min} y_{CO_2}^{Min} \tag{12}$$

$$\dot{n}_H^{Atot(ox)} = \dot{n}_H^{Cout} - \dot{n}_H^{Min} + \dot{n}_H^{Ctot} \approx 2\left(\dot{n}^{Cout} y_{H_2O}^{Cout} - \dot{n}^{Min} y_{H_2O}^{Min}\right) \tag{13}$$

where $\dot{n}_e^{Atot(ox)}$ is the flux of elements due to anodic leakage after complete oxidation of flammable substances. Simplification of Eqs. (12) and (13) is reasonable, as $\dot{n}_C^{Ctot}, \dot{n}_H^{Ctot} \ll \dot{n}_C^{Atot}$, $\dot{n}_H^{Atot}$. The $\dot{n}^{Cout}$ flow rate in Eqs. (12) and (13) is calculated using the nitrogen balance between the module inlet and the cathode outlet, as in:

$$\dot{n}^{Cout} = \frac{\dot{n}^{Min} y_{N2}^{Min} - \dot{n}_{N_2}^{Ctot} + \dot{n}_{N_2}^{Atot}}{y_{N2}^{Cout}} \cong \frac{y_{N2}^{Min}}{y_{N2}^{Cout}} \dot{n}^{Min}, \quad \text{where } y_{N2} = 1 - \sum_j y_j \tag{14}$$

where $j = CO_2, H_2O, O_2$. The simplification of Eq. (14) is reasonable, since $\dot{n}_{N_2}^{Min}, \dot{n}_{N_2}^{Cout} \gg \dot{n}_{N_2}^{Ctot}, \dot{n}_{N_2}^{Atot}$.

The distinction between the viscous and diffusive leakage in the system is done by comparing independently measured HC-ratios of the anodic leakage to each other, according to Eqs. (15) and (16).

$$HC^{Atot,a} = \frac{Y_H^{Atot,a}}{Y_C^{Atot,a}} = \frac{4y_{CH_4}^{Atot,a} + 2y_{H_2}^{Atot,a} + 2y_{H_2O}^{Atot,a}}{y_{CH_4}^{Atot,a} + y_{CO}^{Atot,a} + y_{CO_2}^{Atot,a}}, \quad \text{where } a = diff,\ visc \tag{15}$$

$$HC^{Atot(ox)} = \frac{\dot{n}_H^{Atot(ox)}}{\dot{n}_C^{Atot(ox)}} \tag{16}$$

It should be noted that the HC-ratio in Eq. (15) is obtained with fuel system measurements and the leakage models, while only air system measurements are used for Eq. (16).

2.4.5 Quantification of Leakages

Once the prevailing leakage mechanism has been identified, the anodic leakage is quantified as Eq. (17).

$$\dot{n}^{Atot} = \frac{\dot{n}_C^{Atot}}{Y_C^{Atot,a}} = \frac{\dot{n}_C^{Atot(ox)}}{\left(y_{CH_4}^{Atot,a} + y_{CO}^{Atot,a} + y_{CO_2}^{Atot,a}\right)}, \quad \text{where } a = diff,\ visc \tag{17}$$

Eq. (17) is based on Eq. (6) for the mass balance of carbon.

Quantification of cathodic leakage $\dot{n}^{Ctot}$ is done using Eq. (18).

$$\dot{n}^{Ctot} = \frac{\frac{\dot{n}_C^{Ain} - \dot{n}_C^{Atot}}{Y_C^{Aout}} y_{N_2}^{Aout} - \dot{n}_{N_2}^{Ain} + \dot{n}^{Atot} y_{N_2}^{Atot}}{0.79} \tag{18}$$

where $y_{N_2}^{Atot} = 0$ for diffusive anodic leakage. Eq. (18) is based on Eq. (8) for both nitrogen and carbon balances between *Ain* and *Aout*.

2.5 Uncertainty Analysis

The propagation of the uncertainty of the calculated variables due to the measurements (Table 1) and the inlet natural gas composition (Table 2) is evaluated using Eq. (19):

$$\sigma_y = \sqrt{\sum_{i=1}^{n} \left(\frac{\partial f}{\partial x_i} \sigma_{x_i}\right)^2}, \quad y = f(x_1, \ldots, x_n) \tag{19}$$

where σ_y is the uncertainty of the calculated value y, and σ_{x_i} is the uncertainty of the measured value x_i. Due to large number of measurements (x_i) it is necessary to use symbolic math software to obtain the partial derivates for Eqs. (4)–(18) and calculate their uncertainties numerically. The error bars in all the figures and tables in this manuscript depict either σ_X of a calculated value according to (19), or uncertainty related to the measurement according to Table 1.

3 Results and Discussion

3.1 Air System Measurement Results

Figure 3a–c depicts measured air system gas composition at *Min*, *Cin*, and *Cout* at the time of periodic gas sampling. It is seen that both CO_2 and H_2O fraction at the cathode increases

from the module air inlet to the cathode outlet. These changes can be associated to anodic leakages, since there is no other supply of such substances into the air system. Thus, changes in gas composition between the sampling locations *Min* to *Cin*, *Cin* to *Cout*, and *Min* to *Cout* manifest the effects of the leakages *Aext*, *Aint*, and *Atot*, respectively (see Figure 2), and thus can be used to obtain the HC ratio for any of these leakages, using Eqs. (12)–(14).

The CO_2 and O_2 fractions at *Min* remain nearly constant at approximately 400 ppm and 21.2 vol-%, respectively, while the H_2O fraction varies between 1,000 to 6,000 ppm, according to the prevailing ambient conditions. Compared to *Min*, the measurements at *Cin* show a significant increase for both CO_2 and H_2O, and a much smaller decrease for O_2. The small decrease of O_2 fraction can be associated to the combustion of flammable substances (CH_4, CO, and H_2) of *Aext*, which consume oxygen, and to depletion of air due to *Cext* leakages. However, this small change in the O_2 fraction can be associated to the rather large uncertainty of the O_2 sensor as well.

Similarly, compared to *Min*, even a larger increase for H_2O and CO_2 is evident in *Cout* measurements (Figure 3a–b), due to internal anodic leakages *Aint*, which suggests that *Aint* leakage is of higher magnitude than *Aext*. The O_2 fraction at *Cout* (Figure 3c) is now significantly decreased, mainly due to the utilization of oxygen in the fuel cell reactions.

Generally, due to the high uncertainty associated with the oxygen measurement, quantification of the air leakages cannot be done reliably using air system gas analysis. However, this is not the case for the H_2O and CO_2 measurements – the fuel leakage is significant enough to generate a difference in the measured values that is greater than the sensors' uncertainty, which enables the use of Eqs. (12) and (13) to resolve the element fluxes of the anodic leakage.

3.2 Fuel System Measurement Results

Measured dry fuel gas composition at *Ain* and *Aout* is presented in Figure 4. The total fraction of C_{2+} hydrocarbons was

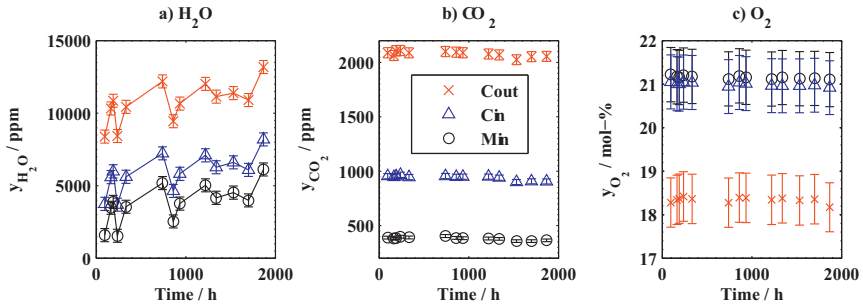

Fig. 3 Measured fraction of a) H_2O, b) CO_2, and c) O_2 in the cathode gas at (○) module inlet *Min*, (△) cathode inlet *Cin* and (×) cathode outlet *Cout*. System at nominal operating conditions with stack current at 200 A.

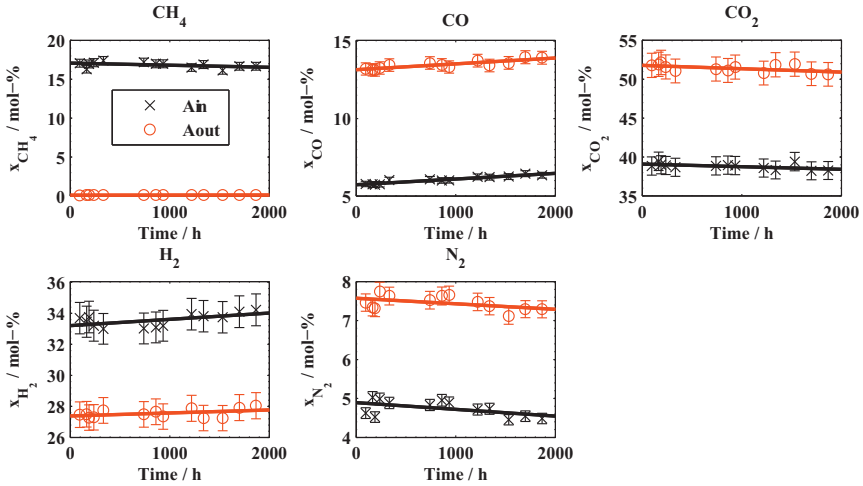

Fig. 4 Measured composition of (×) *Ain* and (○) *Aout* gas on a dry basis. A linear fit is shown as a solid trend line. System at nominal operating conditions with stack current at 200 A.

below 35 ppm for x^{Ain} and below detection limits for x^{Aout}. Figure 4 shows that fuel system gas composition remains relatively stable during the experiment, as the system is operated constantly at nominal operating conditions. According to the first-order linear fit on the measurements, a small trend over time is observed for nearly all gas components. The trend can be related to the temperature increase of the stack during the experiments, which changes gas composition according to the thermodynamic equilibrium.

The wet gas composition at *Ain* and *Aout*, calculated according to Appendix A, is depicted in Figure 5. The wet gas composition is needed to resolve the composition of the anodic leakage in Eqs. (10) and (11), and to quantify the anodic and cathodic leakages according to Eqs. (17) and (18). Similarly to the dry gas composition, the wet gas composition in Figure 5 remains very stable during the experiment. Only a few qualitative observations can be made by inspecting the changes between *Ain* and *Aout*; for example: (i) nearly all methane is reformed in the stack as the y^{Ain}_{CH4} is < 0.1 mol-%; and (ii) cathodic leakages are present in the system, since $y^{Aout}_{N2} > y^{Ain}_{N2}$ and if no cathodic leakages occur then $y^{Aout}_{N2} < y^{Ain}_{N2}$, as all methane is reformed and thus the molar flow at *Aout* is larger than at *Ain*.

3.3 Determination of Prevailing Leakage Mechanism and Quantification of Leakages

The prevailing mass-transport mechanism of the anodic leakage is determined by utilising the independent measurements from the fuel and air subsystems. The leakage models in Eqs. (10) and (11) produce different gas compositions and HC-ratios for the leaking fuel gas. By comparing the HC-ratios obtained (i) with Eq. (16) using air system measurements, and (ii) with Eq. (15) using fuel system measurements and the two leakage models, the leakage mechanism can be determined.

The HC-ratio can be assessed intuitively, even without any analysis results from the fuel system: as the natural gas (mostly CH_4) is the prevailing supply of H and C in the fuel system, then the HC-ratio of the gas in any location of the fuel system should be nearly identical to the inlet natural gas HC ratio of approximately 4. Therefore, if the anodic leakages occur in a viscous manner, a corresponding value of approximately 4 should result for $HC^{Atot(ox)}$ in Eq. (16) as well, regardless of the actual location of the leakage paths within the stack or its manifolds. However, if $HC^{Atot(ox)}$ differs from the inlet natural gas HC-ratio, then the leakage is not occurring viscously, meaning that the composition of the anodic leakage differs from the composition of the fuel gas flowing through the stack.

Figure 6 depicts the HC-ratios obtained by air and fuel system measurements and the two leakage models. The HC-ratios in Figure 6a are calculated with *Ain* gas composition, and in Figure 6b with *Aout* composition, which represent the two extremes in the gas distribution within the stack. It is observed in Figure 6a–b that the HC-ratios given by the viscous leakage model ($HC^{Atot,visc}$) are approximately 4, which are sensible

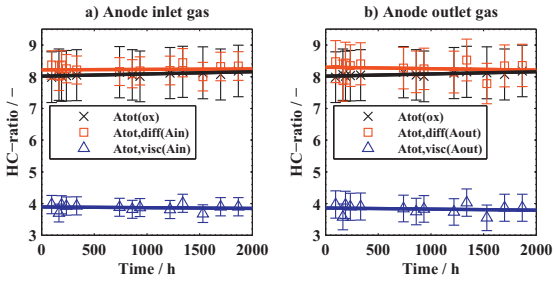

Fig. 6 HC-ratio of the anodic leakage determined by (×) air system measurements, (□) diffusive leakage model, and (△) viscous leakage model, with a) *Ain* and b) *Aout* gas composition. A linear fit is shown as a solid trend line.

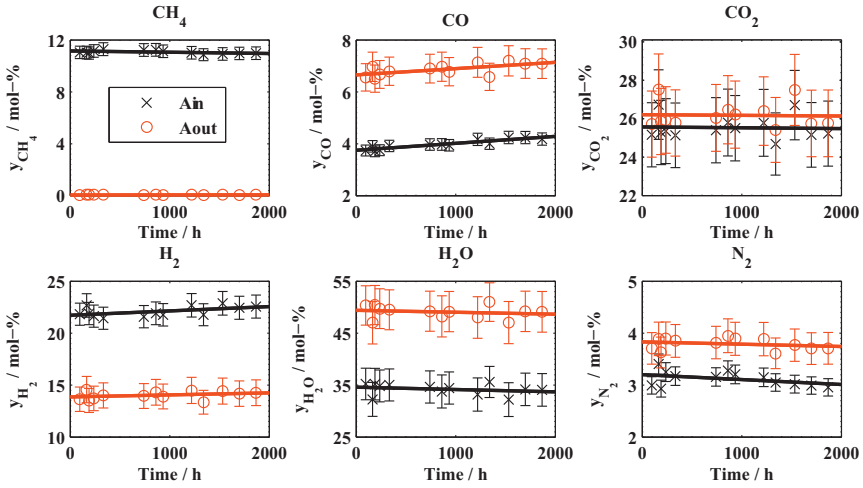

Fig. 5 Composition of the (×) *Ain* and (○) *Aout* gas on a wet basis. A linear fit is shown as a solid trend line.

values that correspond to the properties of the inlet natural gas. However, $HC^{Atot(ox)}$ is approximately 8, which proves that the anodic leakage is not viscous. On the contrary, HC-ratios given by the diffusive leakage model ($HC^{Atot,diff}$) correspond very well to $HC^{Atot(ox)}$. Additionally, within the calculation uncertainty, the HC-ratios for *Aint* and *Aext* leakages are the same as for *Atot* leakage (results omitted for brevity), demonstrating a diffusion-type mass-transfer for both external and internal anodic leakages.

Quantification of the total diffusive anodic and cathodic leakages is now possible using Eqs. (17) and (18), and the results are depicted in Figure 7. Anodic leakages constitute approximately 3% of the anode inlet flow, and it is seen that the leak rate is somewhat higher when y^{Aout} is used as a representative value of the fuel gas composition at the anode. Importantly, it is observed that the leakages of the stack do not increase during the experiment, demonstrating that the gas-tightness characteristics of the stack do not deteriorate, but retain initial performance.

3.4 Complete Combustion of the Anodic Leakage

Calculation of the HC-ratio using Eq. (16) assumes complete combustion of anodic leakage, according to Eqs. (1)–(3), before the gas sample extraction locations in the air system. Incomplete combustion could induce a significant error in the calculated HC-ratio, which can in turn hamper identification of the prevailing mechanism of anodic leakage. Importantly, if any significant amount of unburned CO from anodic leakage was present in the air system, an erroneously high value for the HC-ratio would be obtained.

Table 3 presents the fraction of CH_4, CO, and H_2 at *Cin* and *Cout* gas, measured with GCs and FTIR. The fraction of flammable substances is either below the detection limit or present only as trace amounts, thus their combustion is complete or near-to-complete. In order to emphasize the insignificance of the trace amounts of flammable substances, corresponding values are calculated with 8 NLPM anodic leakage without any combustion taking place.

A comparison of the measured and calculated results clearly reveals that effects of the trace amounts of unburned CH_4, CO, and H_2 on the calculation results are negligible. This is important, since it facilitates the use of simple CO_2 and H_2O sensors to detect anodic leakages, instead of more complex GC and FTIR analysis equipment.

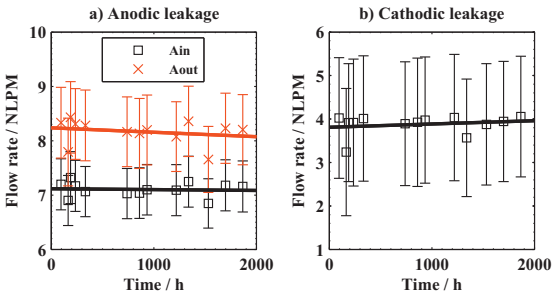

Fig. 7 a) Total anodic leakage calculated using (□) *Ain* and (×) *Aout* gas composition, and b) total cathodic leakage. A linear fit is shown as a solid trend line.

Table 3 Fraction of flammable substances at *Cin* and *Cout*. The measured value and calculated value for an uncombusted anodic leakage are given.

Substance	Unit	Measured		Calculated (uncombusted)	
		Cin	*Cout*	*Cin*	*Cout*
y_{CH_4}	ppm, dry	2	<2	917	893
y_{CO}		2	10	329	321
y_{H_2}		<5	<5	1,828	1,782

3.5 Application of the Analysis Method for System Design and Diagnosis Purposes

The applicability and significance of the developed method for system applications is briefly illustrated next.

3.5.1 System and Stack Design

The presented method can be used to define important operational characteristics for the design of SOFC stacks and systems. To illustrate the applicability of the method, the effects of diffusive anodic leakages on selected important operational characteristics, namely fuel utilization and the additional heat production of the stack, are assessed and discussed. In an ideal case without any leakages, the single-pass fuel utilisation of an SOFC stack in an AOGR system environment can be calculated using Eqs. (20) and (21) [10].

$$FU_{SOFC} = \frac{FU_{SYS}(1-R)}{1-FU_{SYS}R} \tag{20}$$

$$FU_{SYS} = \frac{I}{\sum_j z_j \dot{n}_j^{in} F} \tag{21}$$

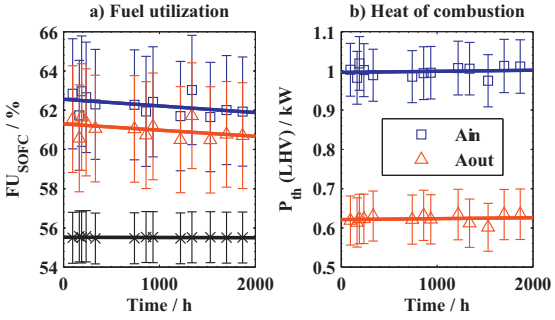

Fig. 8 a) SOFC stack fuel utilisation, and b) heat of combustion due to diffusive anodic leakages with (□) *Ain* and (△) *Aout* gas composition. (×) Ideal fuel utilization without leakages. A linear fit is shown as a solid trend line.

The actual fuel utilization of an SOFC stack, with anodic leakages taken into account, is calculated using Eq. (22). Here, it is assumed the total anodic leakage occurs at the stack inlet manifolds before the anode. Heat produced by complete combustion of the anodic leakages is calculated using Eq. (23).

$$FU_{SOFC}^{leak} = \frac{I}{\left(\sum_j z_j \left(\dot{n}_j^{Ain} - \dot{n}_j^{Atot}\right)\right) F} \tag{22}$$

$$P_{th} = \sum_j \Delta H_j \dot{n}_j^{Atot} \tag{23}$$

Figure 8a depicts both the ideal single-pass fuel utilization of the SOFC stack without leakages (Eq. (20)) and the actual FU with leakages taken into account (Eq. (22)). The results clearly illustrate that the anodic leakages can affect the stack single-pass fuel utilization significantly. The fuel utilization of the stack is increased from approximately 56% up to approximately 62%. It should be noted, however, that Eq. (22) represents the maximum worst-case stack fuel utilization, since all fuel leaks before the anode inlet. In reality, the actual fuel utilization would be lower for the given stack, if leakages are distributed more evenly along the interfaces and occur towards the anode outlet as well. Finally, it is seen that the actual composition of the diffusive anodic leakage will not affect the actual stack fuel utilization significantly, as the difference between the two approximations (i.e. with *Ain* and *Aout* gas compositions) is only approximately 1%-unit.

Combustion of anodic leakages increases the heat production in the stack and its surroundings as depicted in Figure 8b. Here, a diffusive leak approximated by *Ain* gas composition produces more heat, as it contains a higher amount of flammable substances, especially methane. The increased heat production in the stack can be perceived as both a negative and a positive issue with respect to the system operation and design. On the negative side, the increased internal heat production of the stack may require additional cooling - typically accomplished by increasing the cathode air flow rate. Consequently, a penalty to the overall system efficiency is generated as the parasitic power consumption of the air blower increases. On the positive side, leakages may alleviate the need to pre-heat the inlet gas streams using heat exchangers, especially in the case of external anodic leakages, since they will directly heat up the air at the inlet flush. Thus, it may be possible to decrease the size of the air system heat exchangers, which can lower the final cost of the system, provided that the leakages remain the same over the system lifetime.

3.5.2 *Online Diagnosis*

A high enough cross-leakage of hydrogen-containing fuel gas into the air system, for example due to the failure of a seal in an SOFC stack, is detrimental to system reliability and lifetime. The combustion of a leakage concentrated in a specific location is a strong exothermal reaction triggering structural damage, which can in turn increase the leakage and lead to severe equipment failures. Thus, early detection of increased fuel leakages can be beneficial in alleviating the consequences of such failures by using preventive measures such as system shutdown and servicing.

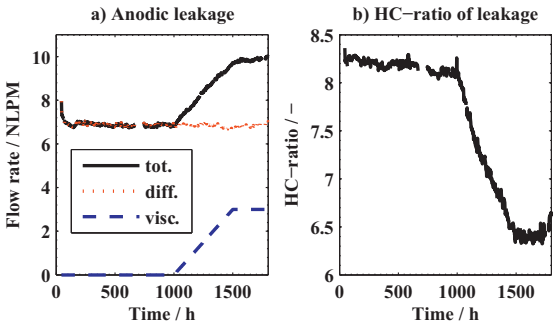

Fig. 9 Simulated case of increasing anodic viscous leakage: a) total anodic (solid line), diffusive (dotted), and viscous (dashed) leakage; b) HC ratio of the total anodic leakage.

The measurement method presented in this study provides means to detect both (i) increases in the absolute amount of leakages, and (ii) changes in the prevailing mass transport mechanism of the leakages. Obviously, any increase of the anodic leakage can be directly detected as an increased flux of carbon and hydrogen in the air system, according to Eqs. (12) and (13). Likewise, the increase of an anodic leakage with a differing mass transport mechanism can be observed as a respective change in the HC-ratio, detectable using the air system measurements, according to Eq. (16). The latter argument is illustrated by a simulated case example, depicted in Figure 9, where a diffusive anodic leakage of approximately 7 NLPM is present in the system, according to the results of this study. A viscous leakage starts to evolve at t = 1,000 h, which can be detected as a progressive decrease of the HC-ratio of the total anodic leakage. Thus, the method presented in this study could be applied, in addition to the general quality assurance for SOFC stacks, for case-specific online fault diagnosis of SOFC systems.

4 Conclusions

In this study, an experimental setup and method is presented to (i) identify the prevailing mass transport mechanism of anodic leakages, and (ii) quantify the anodic and cathodic leakages of an SOFC stack operated in an actual system environment. Identification of the mass transfer phenomenon of anodic leakage cannot be done only by analysing the fuel system's gas composition, but requires measuring the fractions of CO_2, H_2O, and O_2 in the air system, as well as utilization of simple leakage models for diffusive and viscous leakages. Distinction between viscous and diffusive leakages is possible by comparing the HC ratios obtained independently by (i) leakage models and fuel system gas analysis, and (ii) air system gas analysis.

A simple diffusive leakage model provides good correspondence with the HC-ratio calculated directly from the measurement data, and thus it is concluded that the anodic leakages for the given stack occur mainly in a diffusive manner. The effects of diffusive fuel leakages on selected operational characteristics of an SOFC system were studied. Leakages can have negative, but also potentially positive, effects on system design and operation. Importantly, the results of this study demonstrate that the SOFC stack used in the experiments retained its characteristic gas-tightness in a system environment over the whole experiment period, since no changes in either anodic or cathodic leakages were observed.

The experimental method presented in this study was used successfully for *in situ* quantification of leakages during continuous operation of SOFC systems using actual fuel, and without any operational disturbances. Thus, it is possible to utilise the method presented in this study for quality assurance of the SOFC stacks after the manufacturing process, or for fault identification in real-world systems, such as distinguishing a voltage decrease caused by leakages from other degradation mechanisms.

Acknowledgements

Funding for this study was obtained through the projects SofcPower (40074/11) and RealDemo (40076/12). The Finnish Funding Agency for Technology and Innovation (TEKES) and the companies participating in the project are gratefully acknowledged for their financial support. Additionally, M. Halinen would like to thank the following personnel at VTT for their contribution: Kaija Luomanperä and Päivi Jokimies (GC analysis), Hannu Vesala (FTIR analysis), Kari Koskela, Markus Rautanen and Kai Nurminen (help with the experimental setups), and Antti Pohjoranta (manuscript review). Michael Pastula from Versa Power Systems is thanked for his essential contribution related to the stack operability in the 10 kW SOFC system.

Appendix A. Calculation of wet gas composition at anode inlet (y^{Ain}) and anode outlet (y^{Aout})

The solution for y^{Ain} and y^{Aout} is based on the preservation of matter in the elemental flux of the inlet natural gas, recycle, and anode inlet gases (see Figure 2), according to Eq. (A1).

$$\dot{n}_e^{Ain} = \dot{n}_e^{rec} + \dot{n}_e^{in} \tag{A1}$$

We start by defining Eqs. (A2)–(A4), since the fraction of substances in the fuel gas is analyzed from dried fuel gas x^k, for example for H, Eq. (A4) is $X_H^k = 4x_{CH4}^k + 2x_{H2}^k + mx_{CnHm}^k$.

$$\dot{n}^k = \dot{n}_{dry}^k + \dot{n}_{H_2O}^k \tag{A2}$$

$$\dot{n}_{dry}^k = \sum_i \dot{n}_i^k \tag{A3}$$

$$X_e^k = \sum_e A_{e,i} x_i^k \tag{A4}$$

Now, by using Eqs. (A2)–(A4), Eq. (A1) can be written for elements C, O, and H, using separate variables for steam and the remaining substances in the dried gas, as in Eqs. (A5)–(A7).

$$\text{C}: \quad \dot{n}_{dry}^{Ain} X_C^{Ain} = \dot{n}_{dry}^{rec} X_C^{Aout} + \dot{n}_C^{in} \tag{A5}$$

$$\text{O}: \quad \dot{n}_{dry}^{Ain} X_O^{Ain} + \dot{n}_{H_2O}^{Ain} = \dot{n}_{dry}^{rec} X_O^{Aout} + \dot{n}_O^{in} + \dot{n}_{H_2O}^{rec} \tag{A6}$$

$$\text{H}: \quad \dot{n}_{dry}^{Ain} X_H^{Ain} + 2\dot{n}_{H_2O}^{Ain} = \dot{n}_{dry}^{rec} X_H^{Aout} + \dot{n}_H^{in} + 2\dot{n}_{H_2O}^{rec} \tag{A7}$$

Solving (A5)–(A7) for $\dot{n}_{dry}^{rec}$ by eliminating $\dot{n}_{H_2O}^{rec}$ and $\dot{n}_{dry}^{Ain}$, we get Eq. (A8).

$$\dot{n}_{dry}^{rec} = \frac{\dot{n}_C^{in}\left(X_O^{Ain} - 0.5X_H^{Ain}\right) + 0.5\dot{n}_H^{in}\left(X_C^{Ain}\right) + \dot{n}_O^{in}\left(X_C^{Ain}\right)}{X_C^{Ain}\left(X_O^{Aout} - 0.5X_H^{Aout}\right) - X_C^{Aout}\left(X_O^{Ain} - 0.5X_H^{Ain}\right)} \tag{A8}$$

Now, the gas composition on a wet basis at *rec* and *Aout* can be calculated using Eq. (A8), and the measurements for dry gas composition and recycle flow rate using Eqs. (A9)–(A11).

$$\dot{n}_i^{rec} = x_i^{Aout} \dot{n}_{dry}^{rec} \tag{A9}$$

$$\dot{n}_{H_2O}^{rec} = \dot{n}^{rec} - \dot{n}_{dry}^{rec} \tag{A10}$$

$$y_j^{Aout} = y_j^{rec} = \frac{\dot{n}_j^{rec}}{\dot{n}^{rec}} \tag{A11}$$

Similarly, the molar flow rates and gas composition on a wet basis at *Ain* can be calculated using Eqs. (A12)–(A15).

$$\dot{n}_{dry}^{Ain} = \frac{\dot{n}_{dry}^{rec} X_C^{Aout} + \dot{n}_C^{in}}{X_C^{Ain}} \tag{A12}$$

$$\dot{n}_{H_2O}^{Ain} = 0.5\dot{n}_{dry}^{rec} X_H^{Aout} + \dot{n}_{H_2O}^{rec} + 0.5\dot{n}_H^{in} + 0.5\dot{n}_{dry}^{Ain} X_H^{Ain} \tag{A13}$$

$$\dot{n}_i^{Ain} = x_i^{Ain} \dot{n}_{dry}^{Ain} \tag{A14}$$

$$y_j^{Ain} = \frac{\dot{n}_j^{Ain}}{\dot{n}_{dry}^{Ain} + \dot{n}_{H_2O}^{Ain}} \tag{A15}$$

List of symbols

Abbreviations

AOGR	Anode off-gas recycling

Variables and Constants

$\dot{n}$	Flow rate / mol s^{-1} or NLPM
y_j	Fraction of substance j in humid gas / 1
Y_e	Sum of fractions y of element e in humid gas / 1
x_i	Fraction of substance i in dried gas / 1
X_e	Sum of fractions x of element e in dried gas / 1
$A_{e,j}$, $A_{e,i}$	Number of elements e in substance j,i / 1
F	Faraday constant / 96485 C mol^{-1}

FU_{SYS}	System fuel utilization / 1
FU_{SOFC}	SOFC single-pass fuel utilization / 1
R	Recirculation ratio of anode-off gas / 1
z	Number of free electrons in component j / 1
ΔH	Heat of combustion / kJ mol^{-1}

Superscripts

Ain	Anode inlet gas
Aout	Anode outlet gas
rec	Recycle gas
in	System inlet fuel, e.g. natural gas
k	*Ain, Aout, in, rec* process location
Min	Module inlet air
Cin	Cathode inlet air
Cout	Cathode outlet air
Atot	Total anodic leakage
Atot(ox)	Total fully combusted anodic leakage
Atot,visc	Viscous anodic leakage
Atot,diff	Diffusive anodic leakage
Ctot	Total cathodic leakage

Subscripts

e	elements C, H, O, N
j	substances of humid fuel gas C_nH_m, CO, CO_2, H_2, H_2O, O_2, N_2
i	substances of dried fuel gas C_nH_m, CO, CO_2, H_2, O_2, N_2
n	number of carbon atoms in compound
m	number of hydrogen atoms in compound
LHV	lower heating value

Units

NLPM	flow rate in litres per minute at nominal conditions T = 0 °C, p=1013.25 hPa
mol-%	mole fraction as a percentage
ppm	mole fraction as parts per million

6 References

[1] J. W. Fergus, *Journal of Power Sources* **2005**, *147*, 46–47.
[2] J. F. Rasmussen, P. V. Hendriksen, A. Hagen, *Fuel Cells* **2008**, *8 (6)*, 385–393.
[3] M. Powell, K. Meinhardt, V. Sprenkle, L. Chick, G. McVay, *Journal of Power Sources* **2012**, *205*, 377–384.
[4] M. Halinen, O. Thomann, J. Kiviaho, *International Journal of Hydrogen Energy* **2014**, *39*, 552–561.
[5] Z. Wuillemin, N. Autissier, A. Nakajo, M. Luong, J. Van herle, D. Favrat, *Journal of Fuel Cell Science and Technology* **2008**, *5 (011016)*, 1–9.
[6] M. Halinen, M. Rautanen, J. Saarinen, J. Pennanen, A. Pohjoranta, J. Kiviaho, M. Pastula, B. Nuttall, C. Rankin, B. Borglum, *ECS Transactions* **2011**, *35 (1)*, 113–120.
[7] B. Borglum, E. Tang, M. Pastula, *ECS Transactions* **2011**, *35 (1)*, 63–69.
[8] R. J. Kee, E. S. Hetch, G. K. Gupta, H. Zhu, A. M. Dean, L. Maier, O. Deutschmann, *Applied Catalysis A: General* **2005**, *295*, 40–51.
[9] E. N. Fuller, P. D. Schettler, J. C. Giddings, *Industrial and Engineering Chemistry* **1966**, *58 (5)*, 19.
[10] S. Samuelsen, Y. Yaofan, A. D. Rao, C. Brouwer, *Journal of Power Sources* **2005**, *144*, 67–76.

